Pergamon

SCIENCE DIRECT®

Tetrahedron 59 (2003) 9997–10007

TETRAHEDRON

X=Y–ZH system as potential 1,3-dipoles. Part 59: Cascade 1,3-azaprotio cyclotransfer–1,3-dipolar cycloaddition (1,3-APT–1,3-DC) reactions of benzobicyclo[3.3.1]non-5-en-9-one oxime

H. Ali Dondas,[a,b] Colin W. G. Fishwick,[a] Ronald Grigg[a,*] and Mark Thornton-Pett[a]

[a]*Molecular Innovation, Diversity and Automated Synthesis (MIDAS) Centre, Department of Chemistry, The University of Leeds, Leeds LS2 9JT, UK*

[b]*Department of Chemistry, Faculty of Pharmacy, Mersin University, Mersin, Turkey*

Received 28 July 2003; revised 12 September 2003; accepted 9 October 2003

Abstract—Preparation of some novel spiro-oxazolidines related to **3**, which is known to posses anorectic and antidepressant activity, via 1,3-APT–1,3-DC cascades of the oxime of benzobicyclo[3.3.1]non-5-en-9-one **1** is described. Substrate **1** allows the influence of the two bridges on the cascade to be assessed with respect to the configuration of the nitrone that is generated and the facial selectivity of the subsequent cycloaddition.
© 2003 Elsevier Ltd. All rights reserved.

1. Introduction

We have recently reported a range of electrophile induced oxime→nitrone→cycloaddition cascades reactions furnishing nitrones and their cycloadducts in good to excellent yields[1–4] and have previously shown that oximes react with electron deficient alkenes to generate nitrones via a concerted process designated a 1,3-azaprotio cyclotransfer reaction (1,3-APT)[5] (Scheme 1). The resultant nitrones can be trapped in 1,3-DC reactions with either activated or non-activated dipolarophiles. The cascade has four broad synthetic variants (Table 1) and examples of all four variants have been developed.[6,7]

We now report a study of the Class 1 and Class 2 1,3-APT–1,3-DC cascades of the oxime **2** of benzobicyclo[3.3.1]non-5-en-9-one **1**. This substrate allows the influence of the two bridges on the cascade to be assessed with respect to the configuration of the nitrone that is generated and the facial selectivity of the subsequent cycloaddition. Benzobicyclononenone **1**[8] has been utilized as a precursor to amines of type **3** which show anorectic and antidepressant activity.[9,10] A series of bifunctional **4**, **5** and monofunctional **6**, **7** compounds have been evaluated as azaprotiophile and dipolarophile components in reactions with **2** (Fig. 1).

Table 1.

Class	Nitrone formation	Cycloaddition
1	Intermolecular	Intermolecular
2	Intermolecular	Intermolecular
3	Intermolecular	Intermolecular
4	Intermolecular	Intermolecular

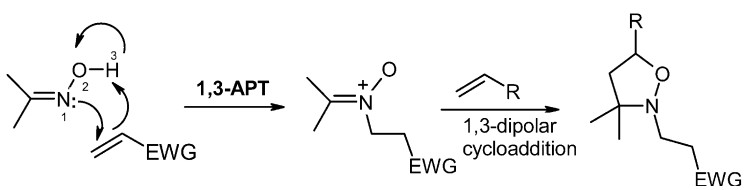

Scheme 1.

Keywords: oxime; nitrone; 1,3-dipolar cycloaddition; 1,3-azaprotio cyclotransfer; spiro-oxazolidines; benzobicyclo; anorectic and antidepressant.
* Corresponding author. Tel.: +44-1-133-436501; fax: +44-1-133-436530; e-mail: r.grigg@chemistry.leeds.ac.uk

0040–4020/$ - see front matter © 2003 Elsevier Ltd. All rights reserved.
doi:10.1016/j.tet.2003.10.027

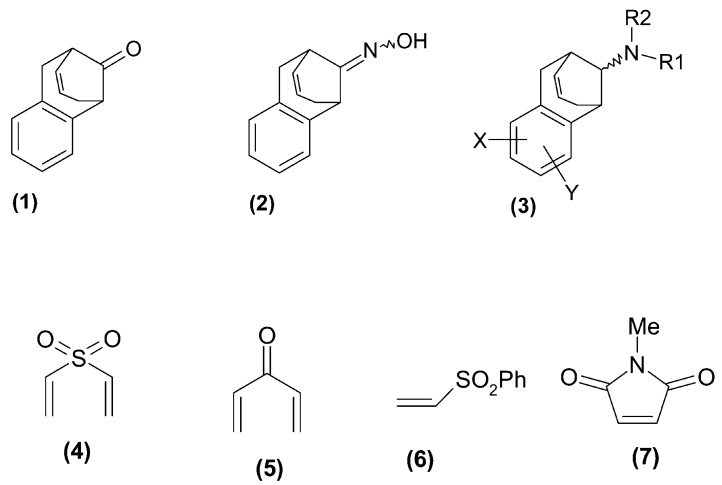

Figure 1.

2. Results and discussion

2.1. Class I processes: intermolecular nitrone formation—intermolecular cycloaddition

2.1.1. Phenyl vinyl sulphone as azaprotiophile/dipolarophile. Oxime **2** was prepared by conventional methods (see Section 4) and found to comprise a 1:1 mixture of *E*/*Z*-isomers. Reaction (toluene, 110°C, 26 h) of oxime **2** with phenyl vinyl sulphone (2 equiv.) furnished cycloadducts **10** and **11** as a 1:1 mixture in 83% yield (Scheme 2). Careful column chromatography on silica allowed the separation of the two isomers. The stereochemistry of **10** and **11** was assigned on the basis of n.O.e data (for data sets see Section 4), 2D-COSY studies and molecular modelling. Thus, in the case of **10**, irradiation of H-10 effected enhancement of the signal for H-3 (12%) and irradiation of H-3 effected enhancement of the signal for H-10 (8%). Irradiation of the H-4 methylene protons effected enhancement of the signal for H-7 (6%) and (CH=CH) (4%). In the case of **11**, irradiation of H-3 effected enhancement of the signals for H-6 (6%), irradiation of H-6 effected enhancement of the signal for H-3 (8%) and irradiation of H-7 effected enhancement of the signal for the Ha methylene protons (7%). This latter n.O.e is diagnostic for cycloaddition *anti* to the propenyl bridge. AM1 calculations show that the two possible nitrones **8** (R=$(CH_2)_2SO_2Ph$, H_f=23.24 kcal mol^{-1}) and **9** (R=$(CH_2)_2SO_2Ph$, H_f=23.51 kcal mol^{-1}) have almost identical energies. These results suggest that cycloadducts **10** and **11** arise from two different nitrones. Product **10** arises from *E*-nitrone **8** via *endo*-cycloaddition *syn* to the propenyl bridge whilst **11** arises

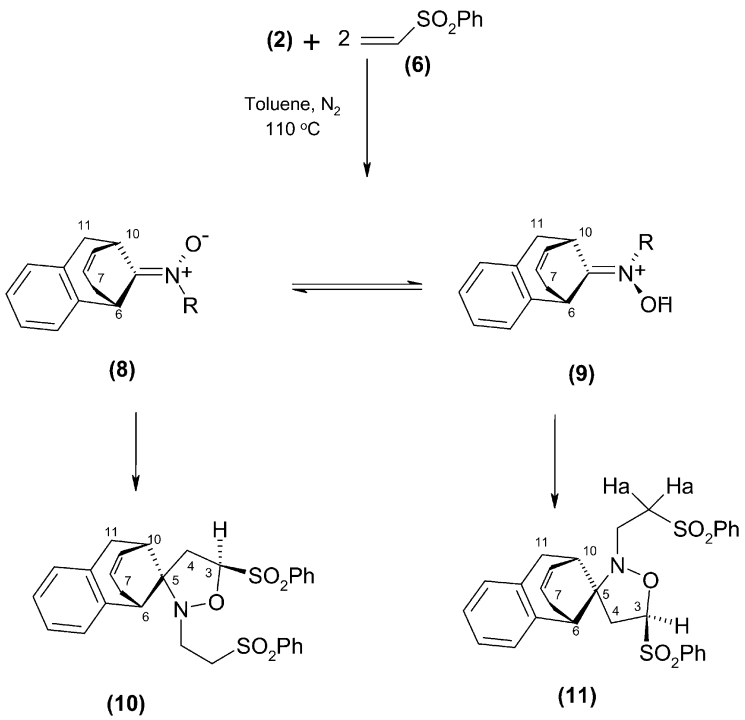

Scheme 2.

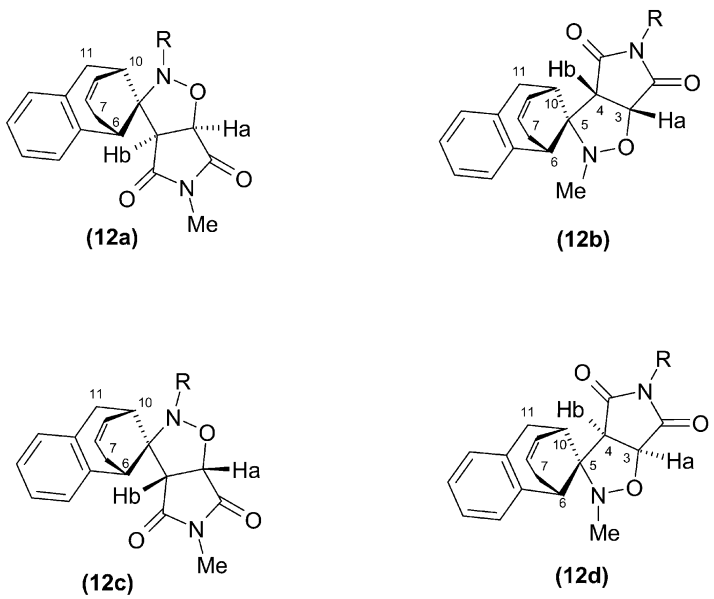

Figure 2.

from *Z*-nitrone **9** via *endo*-cycloaddition *anti* to the propenyl bridge. The assignments of H-6 and H-10 are based on 2D-COSY and n.O.e data (see Section 4).

2.1.2. Chemoselective 1:1:1 adducts. Our attention next turned to examination of the possibilities for chemoselective formation of 1:1:1 adducts of oxime **2**. The key to success in this field lies in identifying two substrates, one of which will function as a good azaprotiophile and a relatively poor dipolarophile, and a second, which will be a reactive dipolarophile and a relatively poor azaprotiophile. In this instance we selected phenyl vinyl sulphone as the azaprotiophile and *N*-methylmaleimide (NMM) as the dipolarophile. When oxime **2** was reacted (toluene, 110°C, 22 h) with phenyl vinyl sulphone (1 mol equiv.) and NMM (1 mol equiv.) it afforded a 1:1 mixture of cycloadducts **12c** and **12d** (R=$(CH_2)_2SO_2Ph$) (Fig. 2). The stereochemical assignments of **12c** and **12d** (R=$(CH_2)_2SO_2Ph$) followed from inspection of their ^1H NMR spectra, 2D-COSY studies, n.O.e. data (for data sets see Section 4), molecular modelling and an X-ray crystal structure of **12c** (R=$(CH_2)_2SO_2Ph$) (Fig. 3). Thus in the case of **12d**, irradiation of Hb-effected enhancement of the signal for H-10 (6%), irradiation of H-10 effected enhancement of the signals for Hb (6%) and Ha (7%) and irradiation of H-7 effected enhancement of the signal for Hb (6%). If, as we believe two nitrones are involved, several mechanistic scenarios can be postulated, and semi-empirical energy calculations have been used to probe these possibilities. Cycloaddition to each nitrone could occur *syn* or *anti* to the propenyl bridge via *endo* or *exo* transition states giving a total of four stereoisomeric cycloadducts **12a–d** (Fig. 2) (Table 2) each of which could arise solely from nitrone **8** or nitrone **9**.

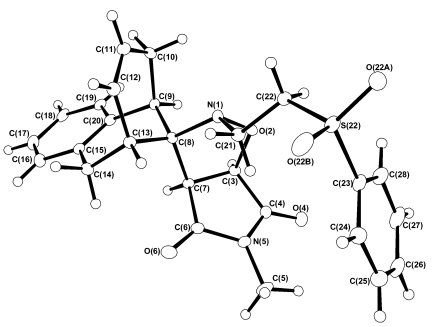

Figure 3. X-Ray crystal structure of **12c**.

Table 2. Cycloadducts resulting from the various modes of cycloaddition

Dipole	Attack *syn*- to propenyl bridge *endo*-t.s.	Attack *syn*- to propenyl bridge *exo*-t.s.	Attack *anti*- to propenyl bridge *endo*-t.s.	Attack *anti*- to propenyl bridge *exo*-t.s.
8	**12d**	**12b**	**12a**	**12c**
9	**12b**	**12d**	**12c**	**12a**

2.2. Mechanism and semi-empirical calculations for Class I processes

The calculated heats of formation of **8** (R=$(CH_2)_2SO_2Ph$, H_f=23.24 kcal mol^{-1}) and **9** (R=$(CH_2)_2SO_2Ph$, H_f=23.51 kcal mol^{-1}) together with their corresponding APT transition states and subsequent activation energies (**2→8**, ΔH=35.21 kcal mol^{-1}, **2→9**, ΔH=35.11 kcal mol^{-1}) indicate that there are no significant energy differences in the 1,3-APT transition states leading to *E*-**8** and *Z*-**9**. Additionally, an estimate of the ease of dipole interconversion via rotation about the C=N bond indicates this to be a relatively high energy process (**8→9**, R=$(CH_2)_2SO_2Ph$, ΔH=49.05 kcal mol^{-1}, **9→8**, R=$(CH_2)_2SO_2Ph$, ΔH=48.78 kcal mol^{-1}).

The cycloaddition preferences for dipoles **8** and **9** with *N*-methylmaleimide were also probed using semi-empirical calculations. To simplify the calculations, and in particular to reduce the conformational flexibility associated with the *N*-ethyl sulphone moiety, these calculations were performed

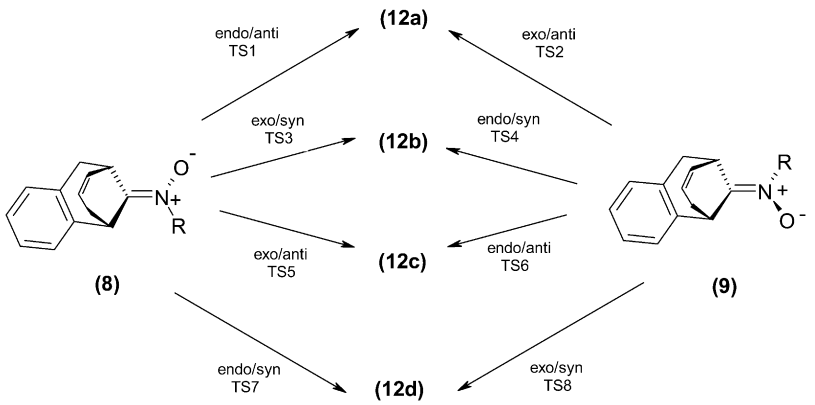

Scheme 3.

Table 3. Calculated heats of formation for hypothetical *N*-methyl 1,3-dipoles and their cycloaddition transition states

Structure (R=Me)	H_f[a]	ν_i[b]	C_5-C_4[c]	O_1-C_3[c]
8	55.41	–	–	–
9	55.46	–	–	–
TS1	50.37	−563.89	2.30	1.92
TS2	55.55	−569.00	2.41	1.89
TS3	53.52	−565.38	2.41	1.87
TS4	49.54	−556.71	2.31	1.91
TS5	54.40	−120.91	2.77	1.54
TS6	46.81	−555.48	2.33	1.90
TS7	46.34	−554.46	2.33	1.90
TS8	53.53	−117.36	2.78	1.54

[a] Heats of formation in kcal mol^{-1}, obtained using AM1 Hamiltonian after full geometry optimisation.
[b] All transition structures were characterized by observing them to have a single negative vibrational frequency corresponding to the reaction coordinate following a normal mode analysis (expressed in cm^{-1}).
[c] Bond length in angstroms.

on the *N*-methyl analogues (**8** and **9**, R=Me). The heats of formation of these together with those of all possible transition states **TS1**–**TS8** leading to the corresponding cycloadducts (**12a**–**d**, R=Me) are summarised above (Scheme 3 and Table 3). Additionally, the corresponding activation energies for the various cycloadditions are summarised in Table 4.

These data indicate that, as in the case for the *N*-(phenylsulphonyl)ethyl dipoles, the *N*-methyl systems **8** and **9** (R=Me) also have essentially identical heats of formation (Table 3). Inspection of the data in Table 4 reveals that, in keeping with our experimental observations, out of the four possible stereoisomeric cycloadducts, **12c** and **12d** are clearly favoured by up to 8 kcal mol^{-1} compared to the other possible cycloadducts. It would also appear that each of these preferred cycloadducts is derived from a particular dipole, **12c** being produced exclusively via cycloaddition of dipole **9** (R=Me), whilst **12d** results from dipole **8** (R=Me). Detailed inspection of the geometries corresponding to each of the transition states **TS1**–**TS8** reveals the origins of these stereochemical preferences. All cases involving an *exo* approach of the dipolarophile are particularly disfavoured (**TS2**, **TS3**, **TS5** and **TS8**). Inspection of the bond lengths for the partially formed single bonds (C_5-C_4, and O_1-C_3, Table 3) for each of these transition structures reveals them to be particularly long. For the cases of **TS5** and **TS8**, the forming bond between C_5 and C_4 appears to be particularly weak as underlined by the very low imaginary vibrational frequencies within these transition states (Table 3). All of these *exo* transition structures involve unfavourable steric interactions between either H_{10} or H_{11} on the dipole and the imide carbonyl and nitrogen atoms from the dipolarophile as the reaction enters into the transition state. Transition state **TS1**, appears disfavoured due to a severe steric clash involving H_b and one of the H_{11} hydrogens which are at a distance of 2.0 Å. Similarly, **TS6** is also disfavoured largely due to the close proximity of H_b and one of the H_7 hydrogens (2.0 Å).

Table 4. Calculated cycloaddition activation energies for hypothetical *N*-methyl 1,3-dipoles

Conversion of **8** and **9** (R=Me)	Transition state	ΔH[a]
8→12a	**TS1**	23.84
9→12a	**TS2**	28.97
8→12b	**TS3**	26.99
9→12b	**TS4**	22.96
8→12c	**TS5**	27.87
9→12c	**TS6**	20.23
8→12d	**TS7**	19.81
9→12d	**TS8**	26.95

[a] Energies in kcal mol^{-1}. This energy is the difference between the sum of the heats of formation of dipole+NMM (H_f=−28.88 kcal mol^{-1}) and the heat of formation of the corresponding transition state.

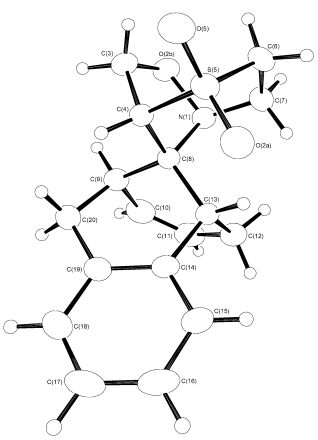

Figure 4. X-Ray crystal structure of **15a**.

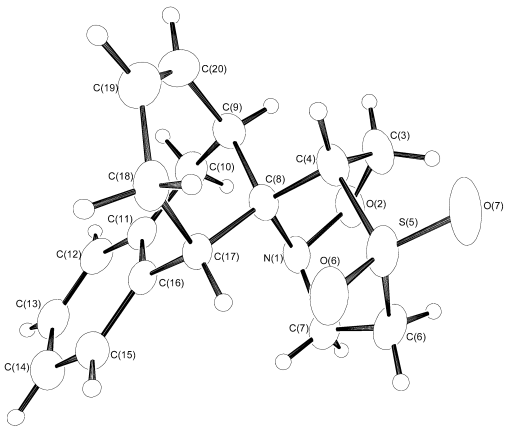

Figure 5. X-Ray crystal structure of **15b**.

2.3. Class II processes: intermolecular nitrone formation—intramolecular cycloaddition

2.3.1. Divinyl sulphone as a bifunctional azaprotiophile/dipolarophile. The 1,3-APT reaction (toluene, 110°C, 24 h) of the benzobicyclononenone oxime **2** with divinyl sulphone as a bifunctional azaprotiophile/dipolarophile furnishes a 1:3 mixture of cycloadducts **15a** and **15b** in 87% combined yield. The structures of both **15a** and **15b** were unequivocally determined by X-ray crystallography (Figs. 4 and 5). Clearly, as in the case for dipole formation in the Class I processes discussed above, in principle two types of dipoles, **13** and **14** possessing either *E*- or *Z*-geometry, can be involved. However, cycloadducts **15a** and **15b** result exclusively from *syn*- and *anti*-cycloadditions within the *E*-dipole (structures **13a** and **13b**) only. We have used semi-empirical calculations to probe the stereo- and regiochemical preferences of this cascade and discuss the mechanistic implications of these studies below (Scheme 4).

2.3.2. Divinyl ketone as a bifunctional azaprotiophile/dipolarophile.[11] An analogous reaction (toluene, 110°C, 28 h) between **2** and divinyl ketone gave a 1:1 mixture (78%) of **18** and **19**. Stereochemical assignments for **18** and **19** are based on by ^{1}H n.O.e and 2D-COSY spectral analysis and by correlation with the products from the corresponding reaction between oxime **2** and divinyl sulphone in which stereochemistry was unequivocally assigned by X-ray crystallography. Irradiation of the H-8 in **18** resulted in enhancement in both H-5 and the *peri*-aromatic hydrogen (8 and 10%, respectively) The X-ray crystal structure of **19** was also determined (Fig. 6, Scheme 5).

2.4. Mechanism and semi-empirical calculations for Class II processes

In order to explore the mechanistic details of the intramolecular cycloadditions, we have applied semi-empirical calculations to both the divinyl sulphone and divinyl ketone based reactions, respectively (Scheme 6). For

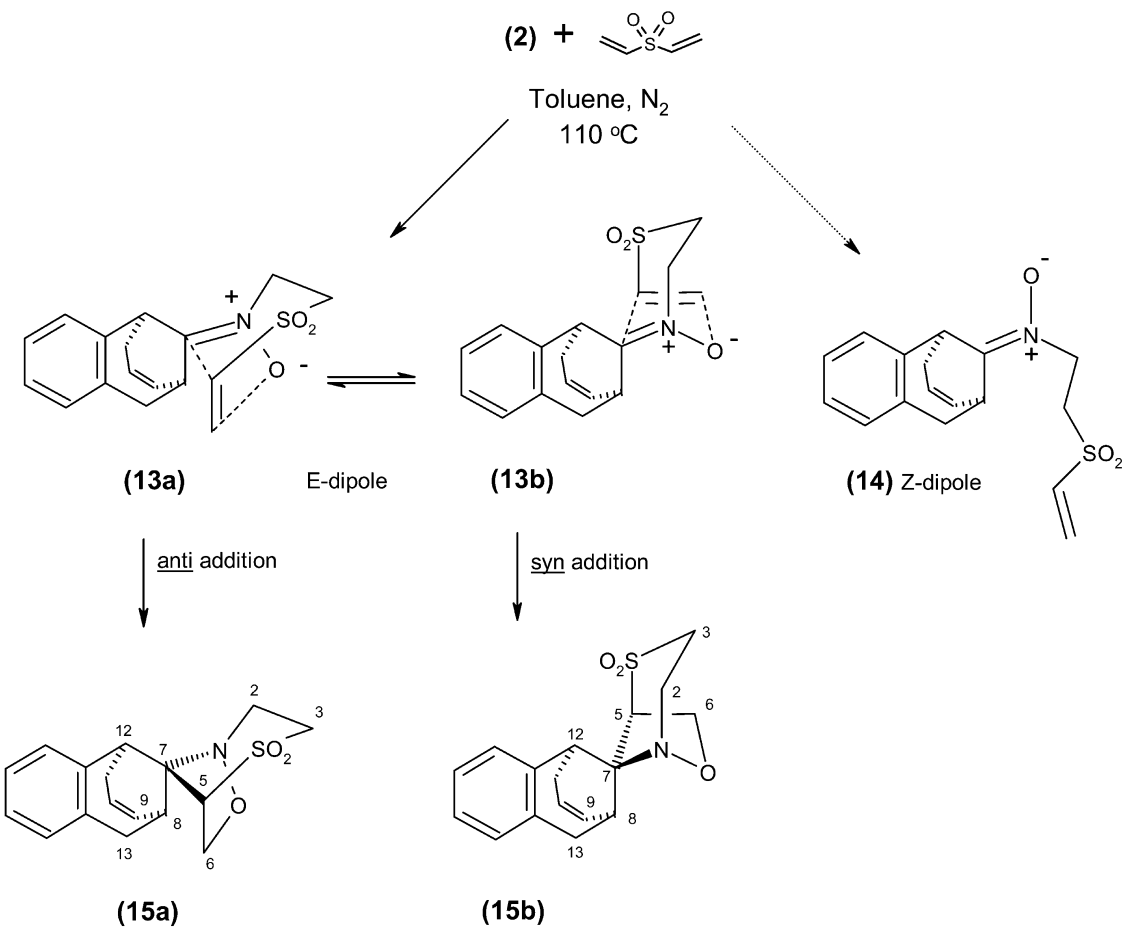

Scheme 4.

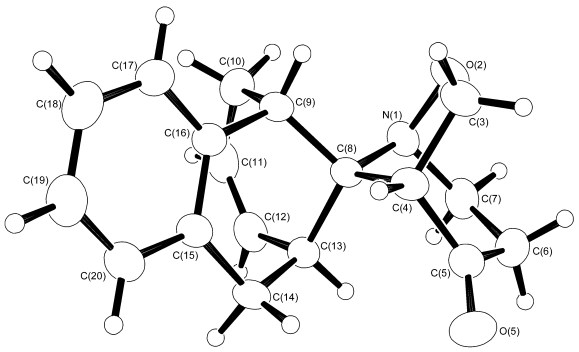

Figure 6. X-Ray crystal structure of (**19**) showing the chair conformation of the N(1)–C(7)–C(8)–C(5)–C(4)–C(8) ring.

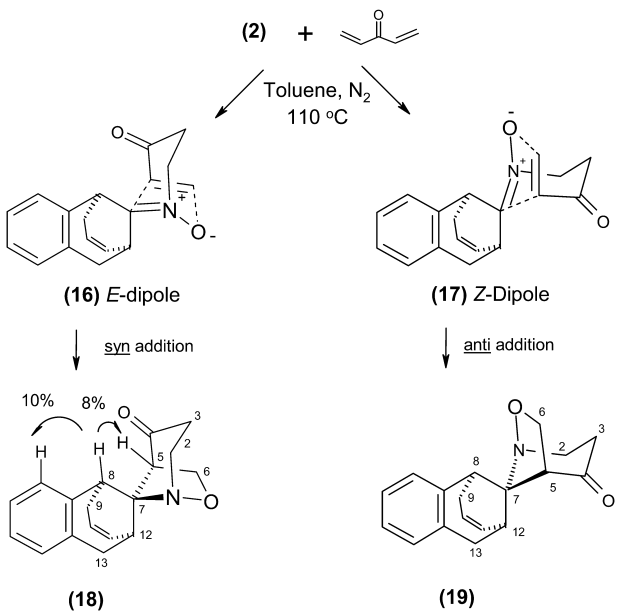

Scheme 5.

the divinyl sulphone-derived systems, as found for the intermolecular cycloadditions described above, the heats of formation for the *E*- and *Z*-dipoles and their corresponding APT transition states were found to be essentially the same and the APT process is predicted to generate both types of dipole geometry. In principle, each dipole can undergo cycloaddition involving four distinct geometries depending on the regiochemistry—here denoted as either *distal* (where the α-carbon within the dipolarophile containing the intramolecular link, bonds to the oxygen of the nitrone), or *proximal* (where the β-carbon of the dipolarophile bonds to the oxygen of the nitrone) (Scheme 6), and stereochemistry of the cycloaddition (with cycloaddition occurring either *syn* or *anti* to the bridging olefin). The structures of all eight possible transition states **TS9**–**TS16** together with their corresponding activation energies (E_a) have been calculated and are summarised in Scheme 3. These data reveal that the activation energies leading to the four transition states involving the *proximal* regiochemistry, **TS11**, **TS12**, **TS15** and **TS16** are markedly lower in energy than the four displaying the alternative *distal* arrangement **TS9**, **TS10**, **TS13** and **TS14**. This would appear to reflect the better alignment of electronic dipoles originating from the carbonyl and nitrone moieties in the *proximal* arrangement. Moreover, the *distal* regiochemistry places one of the H-2 hydrogens and the H-8 hydrogen in very close proximity (less than 1.9 Å) in all four *distal* transition structures **TS9**, **TS10**, **TS13** and **TS14** (**TS9** shown in Figure 7). Additionally, within the four favoured *proximal* arrangements, the calculations reveal a clear preference for transition structure **TS12** (E_a=16.58 kcal mol^{-1}) corresponding to a *syn*-cycloaddition in the *E*-nitrone. This prediction is in keeping with our experimental observations where the major product **15b** results exclusively from **TS12**. However, reaction involving **TS16** is predicted to be only slightly less favourable (E_a=17.90 kcal mol^{-1}), with the activation energies of the remaining *proximal* transition states (**TS11** and **TS15**) less favourable still but similar to each other (21.39 and 20.88 kcal mol^{-1}, respectively). These data would, therefore, predict the formation of lesser amounts of the adduct from cycloaddition involving **TS16** and perhaps also from **TS11** and **TS15**. Although only adduct **15a**, resulting from reaction involving **TS11**, was isolated as the minor product (via crystallisation) from the divinyl sulphone cascade, it is plausible that small amounts of *proximal* adducts resulting from **TS15** and **TS16** were present in the reaction mixture. Calculations on the analogous transition states (**TS17**–**TS24**) from the divinyl ketone-based reactions reveal a very similar trend with the activation energies for reactions involving *proximal* regiochemistry (**TS19**, **TS20**, **TS23** and **TS24**) being substantially lower than those for the *distal* arrangement (**TS17**, **TS18**, **TS21** and **TS22**). Additionally, reactions involving **TS20** (E_a=26.99 kcal mol^{-1}, leading to adduct **18**) and **TS24** (E_a=27.35 kcal mol^{-1}, leading to adduct **19**) have the lowest calculated activation energies, in keeping with our experimental results. However, those of the remaining *proximal* transition structures **TS19** (E_a=29.43 kcal mol^{-1}) and **TS23** (E_a=28.62 kcal mol^{-1}) are only marginally higher and might be expected to give rise to small amounts of the corresponding cycloadducts. Although we cannot rule out the presence of these products in the reaction mixture, it is also possible that these data serve to underline the caution needed when comparing energetically similar calculated activation energies derived from semi-empirical methods with observed product distributions.

2.4.1. Bioactivity. Compounds **12a**, **12b**, **15a** and **15b**, have been assayed in CNS screens for antipsychotic activity against Spiperone binding inhibition of D2 and D3 dopamine receptors. The compounds were inactive compared to the standards Clozapine and Org5222 (70 and 86%, 1 μM and 10 nM, respectively). They showed antifungal activity at 62.5 mg/mL when tested against *Aspergillus fumigatus*. Compounds **15a 15b**, **10**, **11**, **12a**, were inactive when tested against the following: fungi: ERYSGT (wheat powdery mildew), PUCCRT (wheat brown rust), weeds: POAAN (annual meadow grass), insects: DROSME (fruit fly), HELVI (tobacco budworm).

3. Conclusions

We have shown that a series of novel spiro-oxazolidines is readily available via a 1,3-APT–1,3-DC cascade of the oxime of benzobicyclo[3.3.1]non-5-en-9-one. Both

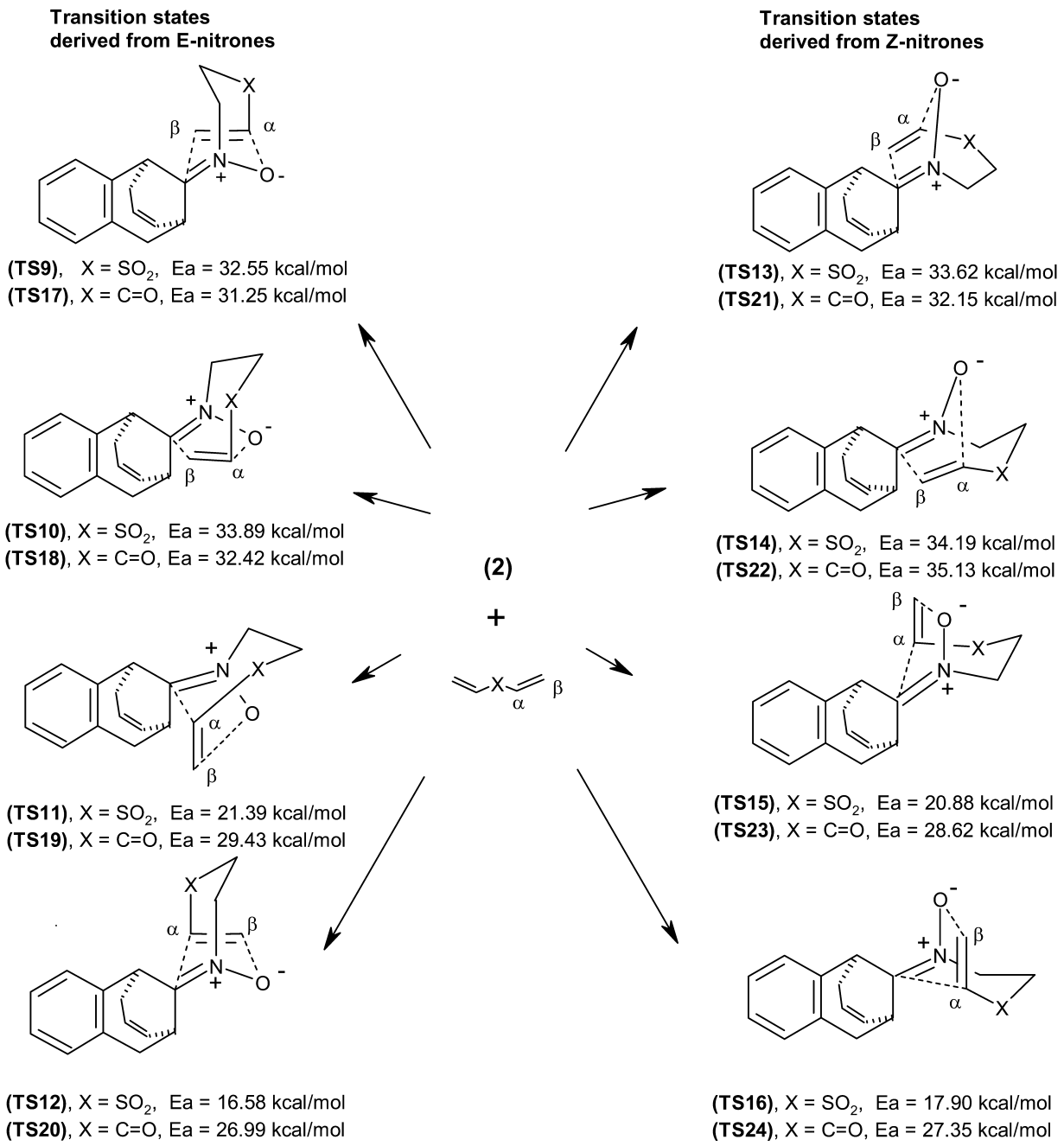

Scheme 6.

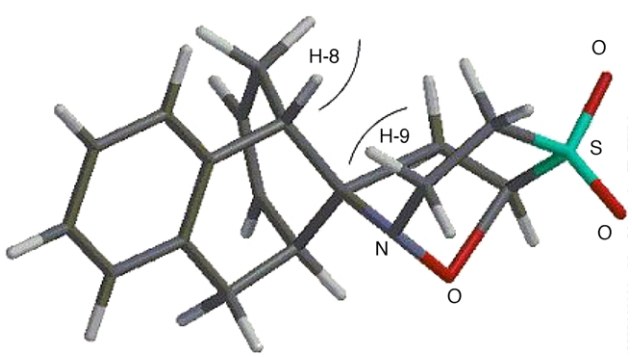

Figure 7.

inter- and intramolecular cycloadditions have been utilised as part of this cascade and the stereoselectivities have been rationalised using semi-empirical calculations. The stereochemical outcome of these reactions originates from a combination of steric and electronic effects in the cycloaddition transition states. Class I cascades involving intermolecular nitrone formation followed by intermolecular cycloaddition, exhibit no selectivity between formation of the *E*- and *Z*-nitrones. The two nitrones react with high *endo* stereoselectivity via either an *anti* (in the case of the *E*-nitrone)- or *syn* (in the case of the *Z*-nitrone) approach of the dipolarophile with respect to the propenyl bridge within the bicyclic framework. The observed stereoselectivities for the Class I processes appear to be the result of a number of

distinct steric clashes within the calculated transition structures. In Class II cascades involving intermolecular nitrone formation followed by intramolecular cycloaddition the nature of the tether exerts a powerful effect on the cycloaddition process favouring the *proximal* regiochemistry. This appears to result from the favourable alignment of electronic dipoles from dipole and dipolarophile, respectively, and also from unfavourable steric interactions in the *distal* regioisomeric arrangement. In the case of divinyl sulphone the 'tether effect' results in the products arising only from the *E* dipole.

4. Experimental

4.1. General

Nuclear magnetic resonance spectra and decoupling experiments were determined at 300 MHz on a QE 300 instrument and at 400 MHz on a Bruker AM 400 spectrometer as specified. Chemical shifts are given in parts per million (δ) downfield from tetramethylsilane as internal standard. Spectra were determined in deuteriochloroform except where otherwise stated. The following abbreviations are used; s=singlet, d=doublet, t=triplet, q=quartet, m=multiplet, br=broad and brs=broad singlet. Flash column chromatography was performed using silica gel 60 (230–400 mesh). Column chromatography employed silica gel GF_{254} (Merck 7730). Petroleum ether refers the fraction with bp 40–60°C unless otherwise specified. Melting points were determined on a Kofler hot stage apparatus and are uncorrected. Microanalyses were obtained using a Carlo-Erba Model 1106 instrument. Mass spectra were recorded at 70 eV on a VG Autospec mass spectrometer.

4.1.1. Benzobicyclonenone oxime 2. A solution of ketone **1** (1.5 g, 8.15 mmol) in acetonitrile (25 mL) and water (15 mL) was treated with hydroxylamine hydrochloride (0.62 g, 8.96 mmol), and sodium acetate (0.8 g, 9.78 mmol) at room temperature overnight. The mixture was then extracted with chloroform (2×50 mL), the combined organic extracts dried ($MgSO_4$) filtered and the solvent removed in vacuo to afford a pale yellow solid. Column chromatography, eluting with 4:1 v/v diethyl ether–petroleum ether afforded the product (1.33 g, 83%) as a 1:1 mixture of *E*/*Z*-isomers as colourless prisms, mp 132–134°C. Found: C, 78.25; H, 6.60; N, 6.95. $C_{13}H_{13}NO$ requires: C, 78.35; H, 6.60; N, 7.05%; δ(300 MHz): 10.22–9.98 (br, 1H, OH), 7.40–7.00 (m, 4H, ArH), 5.64 (m, 2H, CH=CH), 4.62 and 4.21 (2×brs, 1H, CH–C=N) and 3.51–2.02 (m, 4H); *m*/*z*(%): 199 (M^+, 100), 182 (73), 167 (58), 141 (26),128 (85) and 77 (22).

4.1.2. Cycloadducts 10 and 11. A solution of oxime **2** (0.5 g, 2.5 mmol) and phenyl vinyl sulphone (0.84 g, 5.2 mmol) in toluene (40 mL) was stirred under N_2, and held at reflux for 26 h. After cooling the solvent was removed in vacuo and the residue subjected to column chromatography eluting with 3:1 v/v ether–petroleum ether to afford the product (1.12 g, 83%) as a colourless solid comprising a 1:1 mixture of stereoisomers that were separated by column chromatography eluting with 4:1 v/v EtOAc–hexane.

Compound **10**. Crystallised from hexane–DCM as colourless plates, mp 190–192°C. Found: C, 64.30; H, 5.15; N, 2.60; S, 11.75. $C_{29}H_{29}NO_5S_2{\cdot}0.25H_2O$ requires: C, 64.45; H, 5.35; N, 2.60; S, 11.85%; δ(400 MHz.): 7.83–6.96 (m, 14H, ArH), 5.65–5.61 (2m, 2H, CH=CH), 5.00 (t, 1H, *J*=8.5 Hz, H-3), 3.51 (m, 1H, NCH_2S), 3.35 (m, 1H, NCH_2S), 3.12 (dd, 1H, *J*=16.50, 5.8 Hz, H-11), 2.95 (d, 1H, *J*=6.00 Hz, H-6), 2.93 (m, 1H, NCH_2S), 2.75 (m, 2H, H-4 and H-4′), 2.58 (d, 1H, *J*=16.5 Hz, H-7), 2.48 (d, 1H, *J*=16.5 Hz, H-11′), 2.35 (m, 1H, H-10) and 2.2 (dd, 1H, *J*=18.1, 4.4 Hz, H-7′). *m*/*z*(%) (FAB): 536 (M+1, 92), 394 (92), 352 (13), 238 (9), 181 (15), 167 (100) and 141 (30).

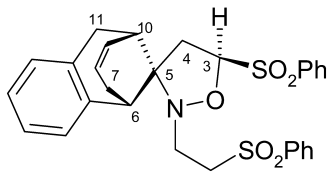

n.O.e. Data. Table 5.

Compound **11**. Crystallised from hexane–DCM as colourless plates, mp 179–181°C. Found: C, 63.1; H, 5.4; N, 2.4 $C_{29}H_{29}NO_5S_2{\cdot}H_2O$ requires: C, 62.9H, 5.45; N, 2.5%; δ (400 MHz.): 7.00–7.96 (m, 14H, ArH), 5.55 (2×m, 2H, CH=CH), 4.95 (t, 1H, *J*=8.0 Hz, H-3), 3.55 (m, 3H, NCH_2S), 3.25 (m, 1H, NCH_2S), 3.00 (dd, 1H, *J*=17.0, 5.5 Hz, H-11), 2.89 (d, 1H, *J*=17.2 Hz, H-11′), 2.80 (d, 1H, *J*=5.5 Hz, H-6), 2.7–2.6 (m, 2H, H-4 and H-7), 2.55 (m, 1H, H-10), 2.4 (dd, 1H, *J*=13.5, 7.5 Hz, H-4′) and 1.85 (dd, 1H, *J*=18.0, 4.3 Hz, H-7′); *m*/*z*(%) (FAB): 536 (M+1, 84), 394 (69), 167 (60), 149 (37), 109 (26), 95 (45), 81 (62) and 69 (100).

Table 5.

		Enhancement (%)								
		H-3	H-4+H-4′	H-6	H-7′	CH=CH	H-10	ArH	NCH′	H-11′
Signal irradiated	H-3		5.8				7.9	6.9		
	H-4+H-4′	15.8		2.4	6.3	3.9	3.3		6.2	
	H-6		3.0		4.4			12.1	5.2	
	H-7		3.3	5.5	26.0	7.3				
	CH=CH				2.5		7.4			
	H-10	11.8	2.0	6.0		11.2				
	NCH		3.9						25.1	
	H-11						8.8	10.2		27.7

Table 6.

	Enhancement (%)											
	H-3	H-4	H-4′	H-6	H-7′	H-7′	CH=CH	H-10	H-11′	SCH	SCH′	ArH
H-3			6.8	6.1								
H-4	2.8			6.1								
H-4′	14.7		20.0									
H-6	8.3											10.2
H-7						9.8	9.7					
H-7′					24.0		8.4					6.3
CH=CH								3.9				
H-11								4.4	11.5			
SCH											8.3	
SCH′										23.13		

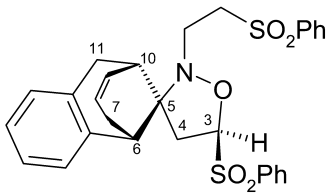

n.O.e. Data. Table 6.

4.1.3. Cycloadducts 12c and 12d. A solution of oxime **2** (0.5 g, 2.5 mmol), phenyl vinyl sulphone (0.42 g, 2.51 mmol) and *N*-methylmaleimide (0.28 g, 2.51 mmol) in toluene (40 mL) was stirred under N_2, and held at reflux for 24 h. After cooling the solvent was removed in vacuo and the residue subjected to column chromatography eluting with 3:1 v/v ether–petroleum ether. The product (1.01 g, 84%) was obtained as a colourless solid that comprised a 1:1 mixture of stereoisomers. The mixture was separated by further careful column chromatography eluting with 4:1 v/v EtOAc–hexane.

Compound **12c**. Crystallised from hexane–DCM as colourless plates, mp 209–211°C. Found: C, 64.35; H, 5.45; N, 5.60 $C_{26}H_{26}N_2O_5S{\cdot}0.5H_2O$ requires: C, 64.05; H, 5.55; N, 5.75%; δ(400 MHz.): 7.9–7.00 (m, 9H, ArH), 5.62–5.53 (br, d, 2H, CH=CH), 4.70 (d, 1H, J=7.50 Hz, Ha), 4.11–4.06 (dd, 1H, J=5.0, 17.5 Hz, H-11′), 3.50 (m, 1H, NCH_2S), 3.35 (m, 1H, NCH_2S), 3.30 (d, 1H, J=7.4 Hz, Hb), 3.27 (m, 1H, NCH_2S), 2.90 (m, 1H, H-11), 2.78 (s, 3H, NMe), 2.8–2.6 (m, 4H, NCH_2S, H-10, H-7′, H-6) and 1.85 (br, d, 1H, H-7); *m*/*z*(%): 478 (M^+, 3), 394 (4), 351 (3), 182 (39), 167 (46), 125 (91), 77 (100) and 51 (55).

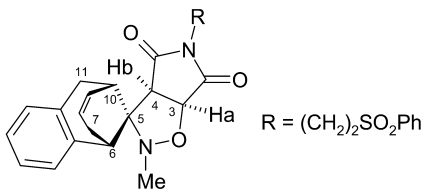

Compound **12d**. Crystallised from hexane–DCM as colourless plates, mp 215–217°C. Found: C, 65.20; H, 5.40; N, 5.85; S, 6.70. $C_{26}H_{26}N_2O_5S$ requires: C, 65.25; H, 5.5; N, 5.85; S, 6.7%; δ(400 MHz.): 7.88–6.98 (m, 9H, ArH), 5.7 (br, 2H, CH=CH), 4.20 (d, 1H, J=7.50 Hz, Ha), 3.68 (d, 1H, J=7.5 Hz, Hb), 3.58 (dd, 1H, J=5.5, 18.5 Hz, H-7), 3.3–3.2 (m, 2H, H-6, H-11′), 3.24 (m, 1H, NCH_2S), 3.00–2.90 (m, 2H, NCH_2S), 2.88 (s, 3H, NMe), 2.75 (m, 1H, NCH_2S), 2.45 (m, 1H, H-10), 2.50 (m, 2H, H-11, Hc) and 2.20 (d, 1H, J=18.5 Hz, H-7′); *m*/*z*(%) (FAB): 479 (M+1, 100), 368 (8), 337 (12), 309 (24), 182 (5) and 77 (9).

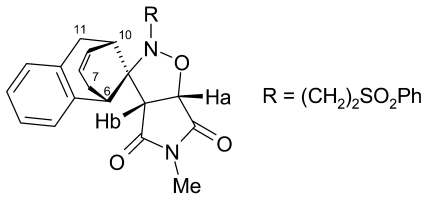

n.O.e. Data. Table 7.

4.1.4. Cycloadducts 15a and 15b. A solution of oxime **2** (0.5 g, 2.5 mmol), and divinyl sulphone (0.3 g, 2.5 mmol) in toluene (40 mL) was stirred under N_2, and held at reflux for 24 h. After cooling the solvent was removed in vacuo. The

Table 7.

		Enhancement (%)							
		Ha	Hb	H-10	H-6′	H-7′	H-11′	ArH	CH=CH
Signal irradiated	Ha		9.8	6.4					
	Hb	13.6		5.8					10.5
	H-10	7.2	5.6				15.9		9.9
	H-6					8.5		12.9	
	H-7		5.5		11.8	37.0			4.6
	H-11						30.0	7.3	
	CH=CH			−5.7		31.5			

^{1}H NMR spectrum of the residue showed it to comprise a 1:3 mixture of **15a** and **15b**. The residue was subjected to column chromatography eluting with 4:1 v/v ether petroleum ether to afford **15a** and **15b** as colourless solids in 87% combined yield.

Cycloadduct **15b**. The product (65%) crystallised from petroleum ether–DCM as colourless prisms, mp 226–228°C. Found: C, 64.00; H, 5.90; N, 4.25; S, 9.95. $C_{17}H_{19}NO_3S$ requires: C, 64.30; H, 6.00; N, 4.40; S, 10.10%; δ(400 MHz): 7.25–7.10 (m, 4H, ArH), 5.7 (br, 2H, CH=CH), 4.62 (d, 1H, J=10.1 Hz, H-6), 4.37 (dd, 1H, J=6.1, 10.1 Hz, H-6′), 3.83 (t, 1H, J=2.8 Hz, H-12), 3.78 (dd, 1H, J=6.0, 2.1 Hz, H-5), 3.35 (m, 4H, H-2, H-2′, H-3, H-3′), 3.1 (m, 2H, H-11 and H-13′), 2.60 (m, 2H, H-8 and H-13) and 2.28 (m, 1H, H-11′); m/z(%): 318 (M+1, 100), 300 (35), 252 (5), 222 (11), 208 (10), 167 (14) and 115 (8).

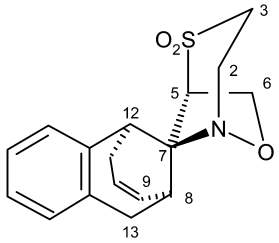

Cycloadduct **15a**. The product (22%) crystallised from petroleum ether–dichloromethane as colourless prisms, mp 213–215°C. Found: C, 64.45; H, 5.75; N, 4.40; S, 9.90. $C_{17}H_{19}NO_3S$ requires: C, 64.30; H, 6.00; N, 4.40; S, 10.1%; δ(400 MHz): 7.35–7.15 (m, 4H, ArH), 5.71 (brs, 2H, CH=CH), 4.61 (d, 1H, J=10.1 Hz, H-6), 4.4 (dd, 1H, J=6.0, 10.0 Hz, H-6′), 4.21 (d, 1H, J=3.0 Hz, H-5), 3.78 (m, 2H, H-12H-13′), 3.4 (m, 2H, H-2, H-3), 3.1–2. 8 (m, 3H, H-13, H-2′, H-3′), 2.7 (brs, 1H, H-8), 2.61 (dd, 1H, J=5.5, 17.5 Hz, H-11) and 2.15 (d, 1H, J=17.6 Hz, H-11′); m/z(%): 317 (M^+, 13), 222 (13), 179 (18), 168 (100), 153 (21), 128 (19) and 115 (20).

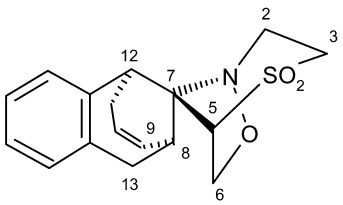

4.1.5. Cycloadducts 18 and 19. A solution of oxime **2** (0. 2 g, 1 mmol) and divinyl ketone (0.09 g, 1.1 mmol) in degassed toluene (25 mL) was stirred under N_2, and held at reflux for 26 h. After cooling the solvent was removed in vacuo. The residue was subjected to column chromatography eluting with 3:1 v/v diethyl ether–petroleum ether to afford a mixture of **18** and **19** (0.219 g, 78%) as a colourless amorphous solid. The isomers were separated by further chromatography on silica eluting with 1:4 v/v EtOAc–hexane.

Compound **18**. Crystallised from hexane–DCM as colourless plates, mp 187–189°C. Found: C, 75.85; H, 6.95; N, 4.75 $C_{18}H_{19}NO_2{\cdot}0.25H_2O$ requires: C, 75.55; H, 6.85; N, 4.9%; δ(400 MHz): 7.26–7.01 (m, 4H, ArH), 5.7 and 5.61 (2×m, 2H, CH=CH), 4.44 (d, 1H, J=7.6 Hz, H-5), 3.5 (m, 2H, H-2 ad H-2′), 3.2 (m, 1H, H-3), 3.05 (d, 1H, J=5.6 Hz, H-8), 2.8–2.6 (m, 4H, H-12, H-6, H-3 and H-13), 2.57 (d, 1H, J=8.7 Hz, H-6β), 2.32 (m, 2H, H-13′ and H-9′), 2.07 (dd, 1H, J=13.4, 2.0 Hz, H-9); m/z(%): 281 (M^+, 71), 181 (36), 167 (100), 152 (26), 141 (22), 115 (29) and 42 (6).

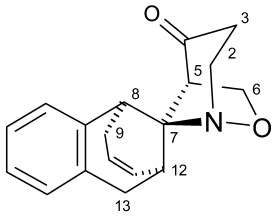

Compound **19**. Crystallised from hexane–DCM as a colourless prisms, mp 181–183°C. Found: C, 76.45; H, 6.95; N, 4.95 $C_{18}H_{19}NO_2$ requires: C, 76.85; H, 6.80, N, 5.00%; δ(400 MHz.): 7.2–7.1 (m, 4H, ArH), 5.66 and 5.60 (2×m, 2H, CH=CH), 4.1 (m, 2H, OCH2), 3.72 (dd, 1H, J=15.0, 10.1 Hz, NCH_b), 3.36 (m, 1H, NCH_a), 3.2 (m, 2H, H-13 and H-8), 3.0 (dd, 1H, J=17.9, 5.4 Hz, H-9′), 2.83 (d, 1H, J=5.2 Hz, H-5), 2.7 (m, 2H, H-3 and H-3′), 2.35 (m, 2H, H-12 and H-13) and 2.06 (dd, 1H, J=16.5, 2.6 Hz, H-9); m/z(%): 281 (M^+, 87), 264 (30), 180 (64), 167 (100), 152 (56), 128 (50) and 115 (55).

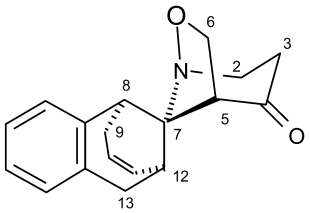

4.2. Single crystal X-ray analysis of 12c, 15a, 15b and 19[12]

All crystallographic measurements were carried out on a Stoe STADI 4 diffractometer at ambient temperature using graphite monochromated Cu K_α X-radiation (λ= 1.54184 Å). Data for all samples were collected in the ranges $4.0<\theta<65°$ using ω/θ scans. No significant variation was observed in the intensity of three standard reflections. Lorentz and polarization corrections were applied to the data sets together with a semi-empirical absorption correction based on azimuthal ψ-scans. The structures were solved by direct methods using SHELXS-86[13] and were refined by full-matrix least squares (based on F^2) using SHELXL-93,[14] which uses all data for refinement.

4.2.1. Crystal data for 12c.[12] $C_{26}H_{26}N_2O_5S$, 0.38×0.32×0.28 mm^3, M=478.55, monoclinic, space group $P21/n$ a=17.084(16) Å, b=13.2325(8) Å, c=20.0329(14) Å, α=90°, β=90.086(5)°, γ=90°, U=4228.8(6) Å^3, Z=8, D_x=1.404 g cm^{-3}, μ=1.623 mm^{-1}, F(000)=2016.

4.2.2. Crystal data for 15a.[12] $C_{17}H_{19}NO_3S$, 0.38×0.28×0.19 mm^3, M=317.39, monoclinic, space group $P21/n$ a=9.8356(2) Å, b=7.7131(3) Å, c=19.8906(4) Å, α=90°, β=99.2980(14)°, γ=90°, U=1489.13(7) Å^3, Z=4, D_x=1.416 g cm^{-3}, μ=2.040 mm^{-1}, F(000)=672.

4.2.3. Crystal data for 15b.[12] $C_{17}H_{19}NO_3S$, 0.55×0.38×0.21 mm^3, M=317.39, monoclinic, space group Pc a=7.9844(6) Å, b=10.9843(7) Å, c=8.7276(6) Å, α=90°, β=103.321(6)°, γ=90°, U=744.84(9) Å^3, Z=2, D_x=1.415 g cm^{-3}, μ=2.040 mm^{-1}, F(000)=336.

4.2.4. Crystal data for 19.[12] $C_{18}H_{19}NO_2$, 0.42×0.37×0.30 mm^3, M=281.34, triclinic, space group P-1 a=7.9484(2) Å, b=13.0733(3) Å, c=14.7801(3) Å, α=90°, β=103.321(6)°, γ=90°, U=1391.27(6) Å^3, Z=4, D_x=1.342 g cm^{-3}, μ=0.693 mm^{-1}, F(000)=600.

Acknowledgements

We thank The University of Leeds, Mersin University, The Scientific and Technical Research Council of Turkey—The Royal Society-UK (TUBITAK-ESEP-Royal Society) and the EPSRC for support.

References

1. (a) Dondas, H. A.; Grigg, R.; Frampton, C. S. *Tetrahedron Lett.* **1997**, *38*, 5719–5722. (b) Dondas, H. A.; Grigg, R.; Thibault, S. *Tetrahedron* **2001**, *57*, 7035–7045.
2. (a) Dondas, H. A.; Cummins, J. E.; Grigg, R.; Thornton-Pett, M. *Tetrahedron* **2001**, *57*, 7951–7964. (b) Dondas, H. A.; Grigg, R.; Markandu, J.; Perrior, T.; Suziki, T.; Thibault, S.; Thomas, W. A.; Thornton-Pett, M. *Tetrahedron* **2002**, *58*, 161–173.
3. (a) Dondas, H. A.; Frederickson, M.; Grigg, R.; Markandu, J.; Thornton-Pett, M. *Tetrahedron* **1997**, *53*, 14339–14354. (b) Markandu, J.; Dondas, H. A.; Frederickson, M.; Grigg, R.; Thornton-Pett, M. *Tetrahedron* **1997**, *53*, 13165–13176.
4. Dondas, H. A.; Grigg, R.; Thibault, S.; Thomas, W. A.; Thornton-Pett, M. *Tetrahedron* **2002**, *58*, 5827–5836.
5. (a) Grigg, R.; Markandu, J.; Perrior, T.; Surendrakumar, S.; Warnock, W. J. *Tetrahedron* **1992**, *48*, 6929–6952. (b) Grigg, R.; Markandu, J.; Surendrakumar, S.; Thornton-Pett, M.; Warnock, W. J. *Tetrahedron* **1992**, *48*, 10399–10422. (c) Dondas, H. A.; Grigg, R.; Hadjisoteriou, M.; Markandu, J.; Thomas, W. A.; Kennewell, P. *Tetrahedron* **2000**, *56*, 10087–10096.
6. (a) Frederickson, M.; Grigg, R.; Rankovic, Z.; Thornton-Pett, M.; Redpath, J.; Crossley, R. *Tetrahedron* **1995**, *51*, 6835–6852. (b) Saba, I. S.; Frederickson, M.; Grigg, R.; Dunn, P.; Levett, P. C. *Tetrahedron Lett.* **1997**, *38*, 6099–6102. (c) Dondas, H. A.; Grigg, R.; Hadjisoteriou, M.; Markandu, J.; Kennewell, P.; Thornton-Pett, M. *Tetrahedron* **2001**, *57*, 1119–1128.
7. (a) Grigg, R.; Heaney, F.; Surendrakumar, S.; Warnock, W. J. *Tetrahedron* **1991**, *47*, 4477–4494. (b) Yokoyama, M.; Sujino, K.; Irie, M.; Yamazaki, N.; Hiyama, T.; Yamada, N.; Togo, H. *J. Chem. Soc., Perkin Trans. 1* **1991**, 2801–2809.
8. We thank Organon Laboratories Ltd., Newhouse, Lanarkshire for a generous gift of ketone (**1**).
9. Hawlett, C. L.; Savage, D. S. British Patent, B.P. 1 504 694, 1978; *Chem. Abstr.* **1976**, *84*, 105298r.
10. Matsuhashi, K.; Shiotani, S. *Chem. Pharm. Bull.* **1970**, *18*, 75–87.
11. (a) Dunn, P. J.; Graham, A. B.; Grigg, R.; Saba, I. S.; Thornton-Pett, M. *Tetrahedron* **2002**, *58*, 7701–7713. (b) Dunn, P. J.; Graham, A. B.; Grigg, R.; Higginson, P.; Saba, I. S.; Thornton-Pett, M. *Tetrahedron* **2002**, *58*, 7715–7725. (c) Dunn, P. J.; Graham, A. B.; Grigg, R.; Higginson, P.; Saba, I. S.; Thornton-Pett, M. *Tetrahedron* **2002**, *58*, 7727–7733.
12. Supplementary data for the X-ray crystallographic studies of **12c**, **15a**, **15b** and **19** including tables of bond lengths and angles have been deposited with the Director of the X-ray Crystallographic Database, Cambridge and are available upon request (**12a**, 191236 CCDC; **14a**, 191237 CCDC; **14b**, 191238 CCDC and **17**, 191239 CCDC).
13. Sheldrick, G. M. *Acta Crystallogr., Sect. A* **1990**, *46*, 467–473.
14. Sheldrick, G. M. *SHELX-93, Program for Refinement of Crystal Structures*; University of Gottingen, 1993.